Primary soot particle distributions in a combustion field of 4 kW pulverized coal jet burner measured by time resolved laser induced incandescence (TiRe-LII)

Nozomu HASHIMOTO*,**, Jun HAYASHI***, Noriaki NAKATSUKA***, Kazuki TAINAKA*, Satoshi UMEMOTO*, Hirofumi TSUJI*, Fumiteru AKAMATSU***, Hiroaki WATANABE*,****, and Hisao MAKINO*

*Central Research Institute of Electric Power Industry
2-6-1 Nagasaka, Yokosuka-shi, Kanagawa 240-0196, Japan
** Hokkaido University
Kita 13, Nishi 8, Kita-ku, Sapporo, 060-8628, Japan
E-mail: nozomu.hashimoto@eng.hokudai.ac.jp
***Osaka University
2-1 Yamadaoka, Suita, Osaka 565-0871, Japan
****Kyushu University
744 Motooka, Nishi-ku, Fukuoka 819-0395, Japan

Received 24 Jun 2016

Abstract

To develop accurate models for the numerical simulation of coal combustion field, detailed experimental data using laser techniques, which can figure out the basic phenomena in a coal flame, are necessary. In particular, soot is one of the important intermediate substances in a coal flame. This paper is the first paper in the world reporting soot particle size distributions in a coal flame. The spatial distribution of the primary soot particle diameter were measured by the combination of the time-resolved laser induced incandescence (TiRe-LII) method and the thermophoretic sampling (TS) method. The primary soot particle diameter distribution was expressed by the log normal function based on the particle diameter measurement using SEM images obtained from the TS samples. The relative function between the signal decay ratio obtained by TiRe-LII and the primary soot particle diameter was defined based on the log normal function. Using the relative function, the spatial distributions of the primary soot particle diameter with the soot volume fraction were obtained. The results show that the small isolated soot regions instantaneously exist in the entire combustion field. This characteristics is different from spray combustion field. From the ensemble-averaged TiRe-LII images, it was found that the soot volume fraction and the primary soot particle diameter increases with increasing the height above the burner in any radial distance. It was also found that the volumetric ratio of small particles decreases with increasing radial distance at the region close to the burner exit. However, the variation of the soot particle diameter distribution along the radial direction becomes small in the downstream region. This tendency is caused by the turbulent mixing effect. It is expected that the accurate soot formation model will be developed in the near future by using the data reported in this paper.

Key words : Coal combustion, Laser induced incandescence, TiRe-LII, thermophoretic sampling, soot particle

1. Introduction

Coal is a very important energy resource for electricity production because of its large reserves compared to petroleum and natural gas. In most coal-fired thermal plants, the coal is utilized using the pulverized coal combustion technology. Even though the basic pulverized coal combustion technology was established many decades ago, there are still many types of problems in the operation of pulverized-coal-fired furnaces, e.g., fouling, slagging and sulfidation

Paper No.xx-xxxx
[DOI: 10.1299/xxx.2014xxx000x]

corrosion. To avoid these problems, the numerical simulation technology have been developed to predict the combustion characteristics in coal-fired boilers (e.g., Kurose et al., 2004, Hashimoto et al., 2007, Aydin and Durak, 2012). Some new models or methods for coal combustion field, e.g., the new devolatilization model (Hashimoto et al., 2012a, 2012b, Hashimoto et al., 2014), the new char combustion model (Umetsu et al., 2014), the skeletal mechanism for the volatile matter combustion (Ahn et al., 2016), the transported PDF model (Zhao et al., 2014), the velocity-scalar joint filtered density function model (Wen et al., 2015), the new heterogeneous combustion model (Vascellari et al., 2014), the large eddy simulation of coal combustion field (Rabacal et al., 2015, Franchetti et al., 2013, Olenik et al., 2015, Muto et al., 2015), have been developed recently. To model the various phenomena in the combustion field for developing the accurate simulation technology, the understandings of coal combustion phenomena are necessary. For this purpose, experimental researches employing the laser techniques have been conducted by some researchers (Hwang et al., 2005, Hayashi et al., 2013, Balusamy et al., 2015). However, there are still various phenomena that are not clarified yet due to the complexity of pulverized coal combustion phenomenon. For instance, the combustion reactions of volatile matter are complex and the detailed intermediate substances have been not clarified yet. One of important intermediate substances is soot particle. However, the mechanism of soot particles formation in the coal combustion field has not been clarified in detail. Recently, our research group applied the laser induced incandescence (LII) technique to the coal combustion field and clarified the location of soot formation region in the small coal jet burner (Hayashi et al., 2013). For the development of the accurate soot formation model in the coal combustion field, however, more detailed information of the soot particles is required. In particular, the soot particle size distribution in a coal flame is important to understand the soot particle growing process in the flame. The soot particle size distribution data in a gaseous fuel combustion field (Sun et al., 2015) and a spray combustion field (Oh et al., 2006) have been obtained employing the time-resolved laser induced incandescence (TiRe-LII). However, the soot particle size distribution in a solid fuel combustion field has not yet been measured.

In this study, the detailed primary soot particle size distributions in a 4 kW small coal jet burner in the Central Research Institute of Electric Power Industry (Hwang et al., 2005) were investigated by employing TiRe-LII method and the thermophoretic sampling (TS). The burner is known as one of the target flames for coal combustion researchers in the world. Various numerical simulation techniques have been applied for this burner (Hashimoto et al., 2012b, Zhao et al., 2014, Vascellari et al., 2014, Franchetti et al., 2013, Stein et al., 2013, Cai et al., 2015, Hara et al., 2015). From the previous studies, the distributions of OH radical (by OH-PLIF) and the velocity and size of coal particles (by SDPA) (Hwang et al., 2005) and the distribution of soot volume fraction (by LII) (Hayashi et al., 2013) of the burner have been reported. This paper is the first paper in the world reporting a soot particle size distribution in a coal flame. The spatial

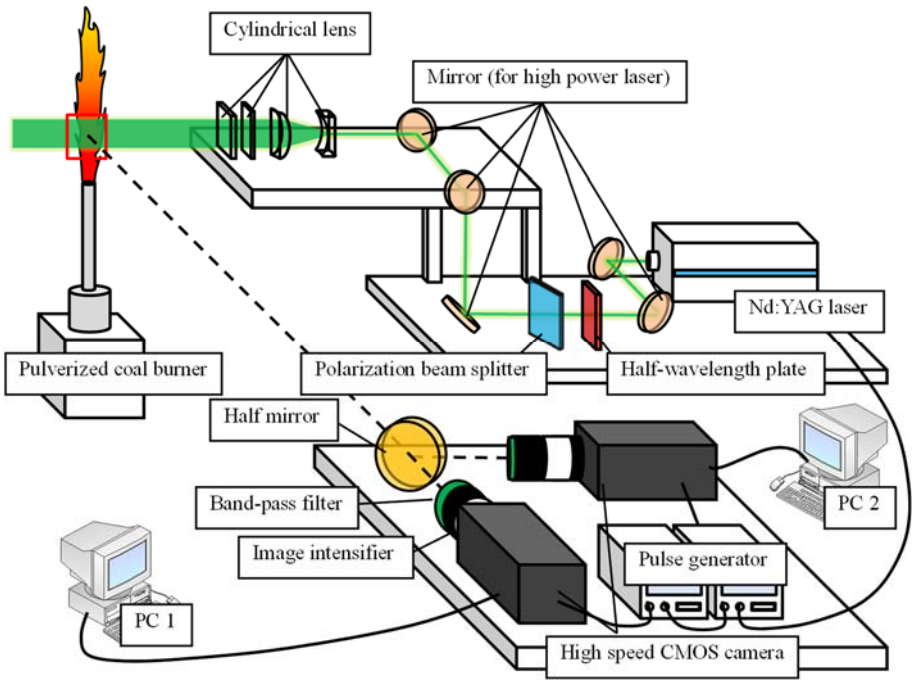

Fig. 1 Schematic illustration of time-resolved laser incandescence (TiRe-LII) measurement system

[DOI: 10.1299/xxx.2014xxx000x]

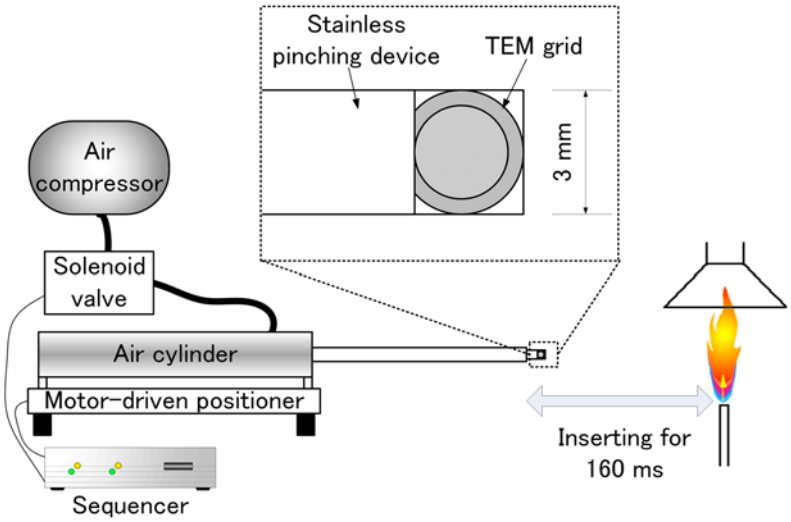

Fig. 2 Schematic of thermophoretic sampling system

distribution of the primary soot particle diameter were measured by using the relative function between the signal decay ratio from TiRe-LII and the primary soot particle diameter distributions from the particle SEM images collected by TS. The experimental data obtained by this study is very useful for the development of the accurate soot formation model in the coal combustion field. The soot formation process is roughly divided into (a) Formation of molecular precursors of soot, (b) Nucleation or inception of particles from heavy PAH molecules, (c) Mass growth of particles by addition of gas phase molecules, (d) Coagulation via reactive particle-particle collisions, (e) Carbonization of particulate material, (f) Oxidation (Richter et al., 2000). By using the primary soot particle size distribution data obtained by this study, the balance of reaction rates for process (c), (d) and (f) in soot formation models for coal combustion fields can be checked in detail.

2. Experimental

In this study, TiRe-LII and TS were applied to a combustion field of a 4 kW small coal jet burner (Hwang et al., 2005) in the Central Research Institute of Electric Power Industry. Figure 1 shows the schematic illustration of the time-resolved laser induced incandescence measurement system.

The second harmonic wave length of Nd:YAG laser (532 nm) was used as a light source. The laser sheets was formed by using four cylindrical lenses with focal lengths of f = 2000 mm, 25 mm, -300 mm and 700 mm. The laser sheet fluence was controlled by the polarization beam splitter and the half-wavelength plate with maximum power output of the laser to keep the same laser sheet profile regardless of the laser fluence. Two high speed CMOS cameras (Phantom V12, Vision Research Co. Ltd.) with image intensifier (C9016-23MOD) and bandpass filter (center wavelength = 400 nm, half bandwidth = 60 nm) were used to detect the incandescence signal from soot particles. The maximum transmission level of the bandpass filter was 70%. To eliminate the light emission from the flame, the gate period was set to 20 ns for both cameras. In addition to that, the open time of the gate for the 1st camera was delayed by 100 ns from the beginning of the laser pulse to eliminate the fluorescence signals of PAHs induced by the laser light. The delay period between the 1st camera and 2nd camera was set to 450 ns to obtain the incandescence signal decay information. As discussed in the previous research (Hayashi et al., 2013), the laser power profile largely affects the LII signal intensity. Therefore, only homogeneous part of the laser sheet was used to evaluate the LII signal in the same as the previous research (Hayashi et al., 2013). In addition to that, the laser fluence was adjusted to appropriate value (0.1 J/cm^2), which is sufficiently high to heat up all the soot particles to the sublimation temperature but also sufficiently low to avoid the incandescence of coal particles. If the laser fluence is much higher than 0.1 J/cm^2, the LII signal will be emitted from not only soot particles but also from coal particles (Hayashi et al., 2013). By adjusting the laser fluence to 0.1 J/cm^2, only the LII signal from soot particles were obtained.

Figure 2 shows the schematic of the thermophoretic sampling system. A transmission electron microscope (TEM) grid was inserted in the flame of the jet burner for 160 ms by using the insertion system equipped with the air cylinder. The insertion period of 160 ms was measured from the movie taken by a high speed camera. Soot particles were adhered

[DOI: 10.1299/xxx.2014xxx000x]

on the surface of the TEM grid by thermophoretic effect with the temperature difference of a hot combustion gas and a cold TEM grid. The deepest position of each insertion was set at the central axis of the burner. Therefore, the grid reached the central axis after passing through the cylindrical shape flame and passed the flame again when the grid was moved to the original position outside the flame. Consequently, the soot particles all over the radial position were corrected by passing through the flame twice. The soot particle samples were observed in detail by using a scanning electron microscope (SEM).

Table 1 and 2 show the properties of coal used in this experiment and the experimental condition. Used coal and the experimental condition are the same as the previous research (Hwang et al., 2005, Hayashi et al., 2013). Figure 3 shows the Rosin-Rammler distribution of coal particles. The mass median diameter is about 40 μm. The structure of the burner is shown in the right-hand side of Fig. 4. Pulverized coal particles were supplied with air from the main burner port with an inner diameter of 6 mm. Methane was supplied from an annular slit with a width of 0.5 mm to maintain a coal flame. The more detailed information about the burner and combustion experiment is available in the paper by Hwang et al. (2005).

Table 1
Properties of coal

Item	Value
Proximate analysis [wt%]	
Moisture[b]	2.60
Ash[a]	15.20
Volatile matter[a]	26.90
Fixed carbon[a]	57.90
Ultimate analysis [wt%]	
Carbon[a]	71.90
Hydrogen[a]	4.40
Nitrogen[a]	1.50
Oxygen[a]	6.53
Total sulfur[a]	0.44
Combustible sulfur[a]	0.39
Lower heating value [MJ/kg]	28.1

[a] Dry basis, [b] As received

Table 2
Experimental condition

Item	Value
Pulverized coal feed rate [kg/s]	1.49×10^{-4}
Thermal input of coal[a] [kW]	4.19
Thermal input of CH_4[a] [kW]	0.83
Air flow rate [m^3/s]	1.80×10^{-4}
CH_4 flow rate [m^3/s]	2.33×10^{-5}
Bulk equivalence ratio, ϕ	6.09
Reynolds number, *Re*	2544

[a] Based on the lower heating value

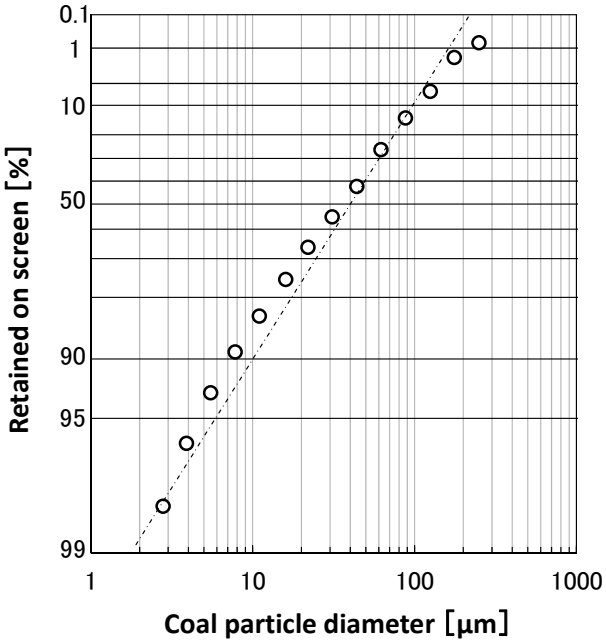

Fig. 3 Rosin-Rammler distribution of coal particles

[DOI: 10.1299/xxx.2014xxx000x]

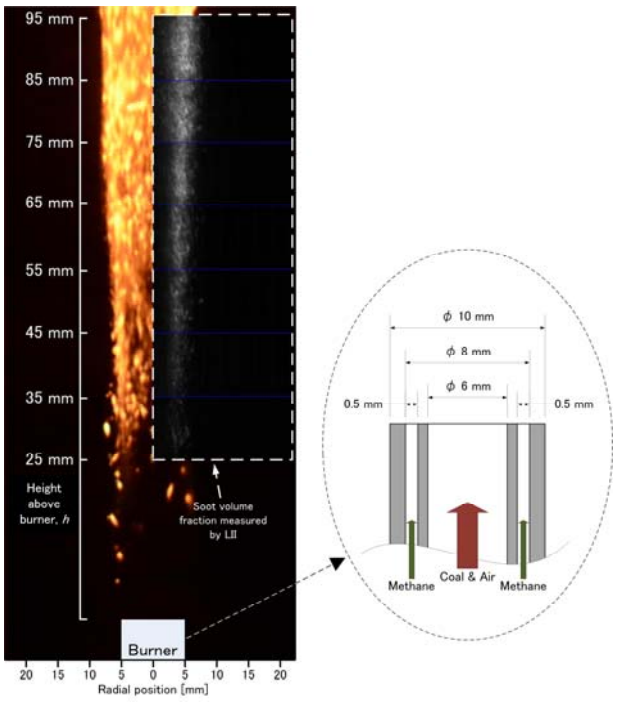

Fig. 4 Direct flame photo and soot volume fraction distribution obtained by LII

3. Results and Discussion

3.1 Soot volume fraction distribution obtained by LII

Figure 4 shows the direct flame photo and the soot volume fraction distribution obtained by LII signal. The measurement method of the soot volume fraction was the same as the previous research (Hayashi et al., 2013), although the camera and the image intensifier were different. The soot volume fraction was obtained by the ensemble average of 500 shots of LII signal. It is found that the region with high soot volume fraction is observed at the outer region of the luminous flame and this trend is consistent with the previous research. It is also found that the soot volume fraction is increased with the height above the burner, *h*. This tendency is consistent with that from SEM images as described in the next section.

3.2 Primary soot particle diameter distributions obtained by TS

Figure 5 shows the typical SEM images of soot particles collected by TS and the cumulative frequency and the probability density functions for primary soot particle diameter based on particle volume. It is observed from Fig. 5 (a-1), (b-1) and (c-1) that the number density of the particles on the sample grid is increased with increasing *h*. This tendency indicates that the number density of the soot particles in the flame increases with *h* (Note that the insertion period of the thermophoretic grid is same for all *h*). This is consistent with the measured soot volume fraction by LII as indicated in Fig. 4.

The diameters of over 1000 primary soot particles in 25 SEM images, which were randomly taken from the grid sample, were measured for each height above the burner, *h*. The solid circles in Fig. 5 (a-2), (b-2) and (c-2) are the cumulative plots of the measured primary soot particle diameters. The solid lines are approximated cumulative curves of primary soot particle diameter employing the log normal function expressed by the following equation.

$$F(D_p) = \frac{1}{2} erfc\left[-\left(\frac{\ln(D_p) - \ln(D_{p,m})}{\sigma\sqrt{2}} \right) \right] \tag{1}$$

[DOI: 10.1299/xxx.2014xxx000x]

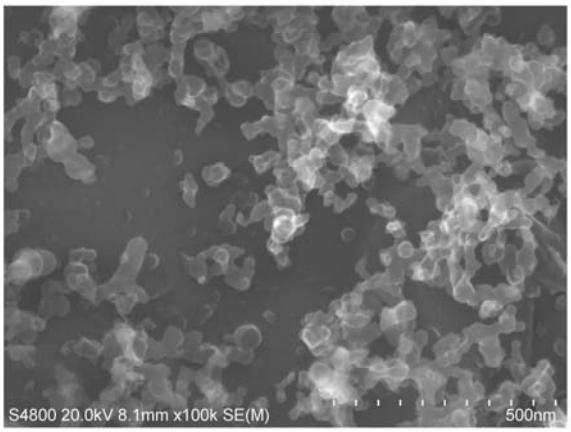

(c-1) Typical image of soot particles sampled at h = 95 mm

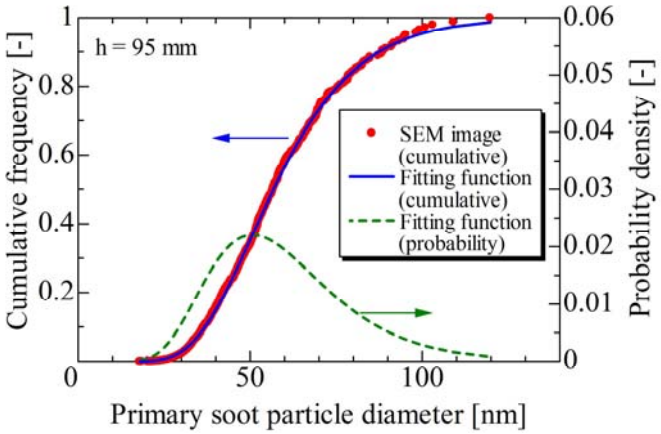

(c-2) Cumulative frequency and probability density functions for primary soot particle diameter (h = 95 mm)

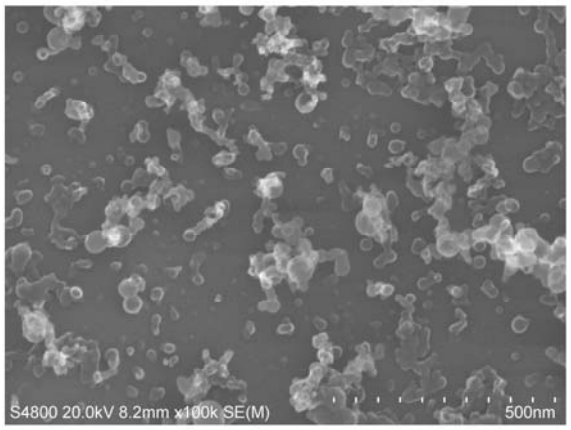

(b-1) Typical image of soot particles sampled at h = 65 mm

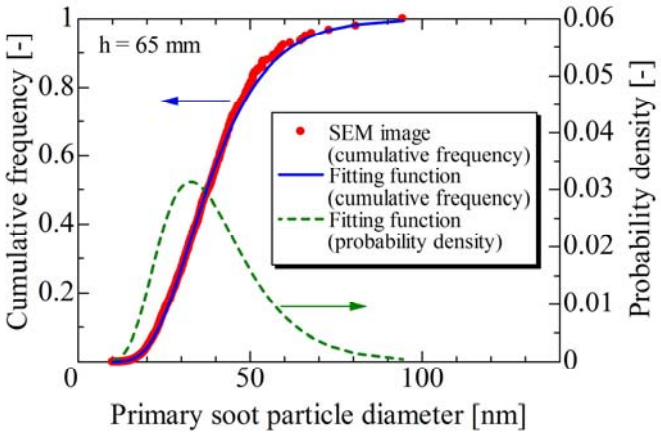

(b-2) Cumulative frequency and probability density functions for primary soot particle diameter (h = 65 mm)

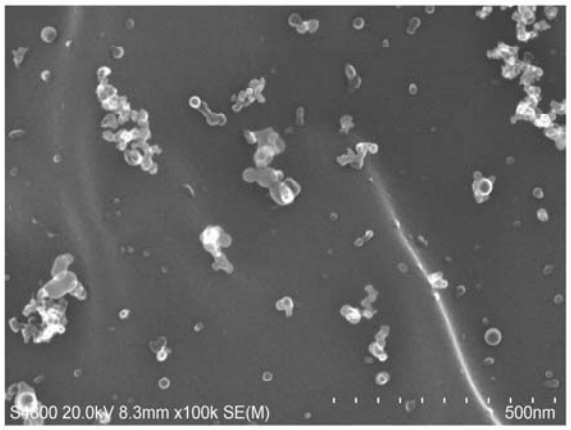

(a-1) Typical image of soot particles sampled at h = 35 mm

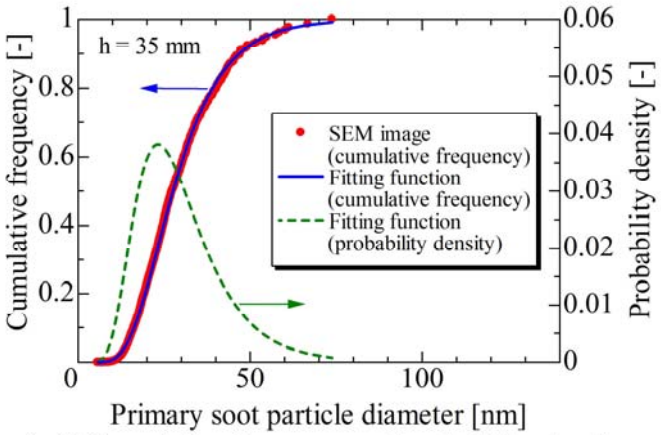

(a-2) Cumulative frequency and probability density functions for primary soot particle diameter (h = 35 mm)

Fig. 5 Typical SEM images of soot particles and cumulative frequency and probability density functions for primary soot particle diameter

where, D_p and $D_{p,m}$ are the primary soot particle diameter and its median diameter based on the particle volume, respectively. The parameter σ and $D_{p,m}$ were determined by the least squares method to fit the curves to the measured diameter distributions. The dotted lines indicate the probability curves converted from the solid lines expressed by the

[DOI: 10.1299/xxx.2014xxx000x]

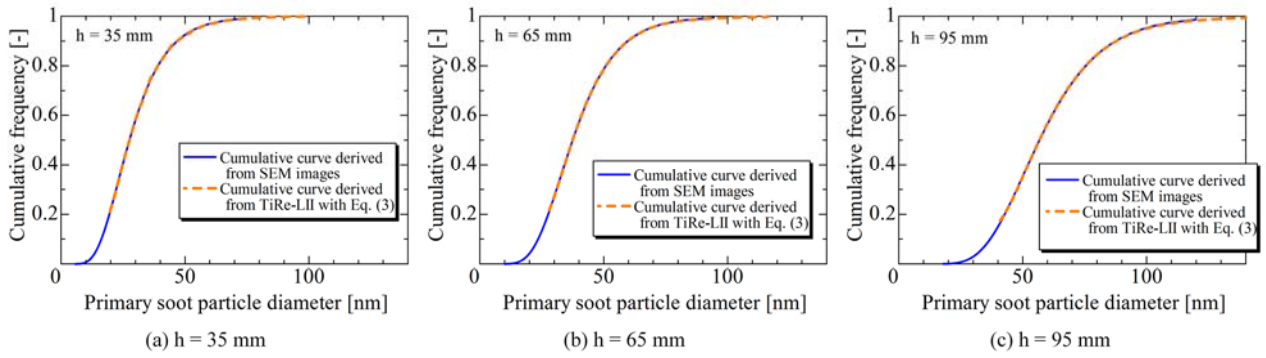

Fig. 6 Cumulative frequencies of primary soot particle diameter obtained from SEM images and obtained from LII signal decay ratio with the fitting function (Eq. (3)).

Table 3
Values of fitting parameter

h	k_1	k_2	k_3
35 mm	80.7	1.05	19.7
65 mm	88.2	1.02	28.0
95 mm	118.6	1.00	40.9

following equation.

$$P(D_p) = \frac{1}{\sqrt{2\pi}\sigma D_p} \exp\left[-\frac{1}{2}\left(\frac{\ln(D_p) - \ln(D_{p,m})}{\sigma} \right)^2 \right] \tag{2}$$

It is observed that the diameter distribution of primary soot particles shifts to larger side with increasing *h*. This tendency indicates the growth of the primary soot particles as the particles move to the downstream region. The growth of the primary soot particles is proceeded by the surface growth by addition of gas phase molecules and coagulation of soot particles. The soot particles can be oxidized by gaseous species such as OH, O and O_2. From the fact that the primary soot particle size increases with h, it is obvious that the growth rate of the primary soot particles is larger than the oxidation rate of soot particles. It is also found that the distribution of the primary soot particle diameter grows wider with increasing *h*, i.e., the peak value of the probability density decreases with increasing *h*. In this study, the spatial distribution of the primary soot particle diameter in the flame was analyzed by the combination of the diameter distribution data in Fig. 5 and the TiRe-LII signal data as presented in the next section.

3.3 Spatial primary soot particle diameter distributions obtained by TiRe-LII

The relative function between the signal decay ratio obtained by the TiRe-LII and the primary soot particle diameter was defined by the following equation so that the primary soot particle cumulative function obtained from the TiRe-LII signals is consistent with that obtained from the thermophoretic sampling (Eq. (1)).

$$D_p = k_1 S^{k2} + k_3 \tag{3}$$

where *S* is the signal decay ratio between the 1st and 2nd cameras during the TiRe-LII measurement, k_1, k_2 and k_3 are fitting parameters. The values of k_1, k_2 and k_3 are listed in Table 3.

Figure 6 shows the comparison of the cumulative frequency curves of primary soot particle diameter obtained from SEM images and obtained from LII signal decay ratio *S* with the Eq. (3). By employing the fitting function, the primary

[DOI: 10.1299/xxx.2014xxx000x]

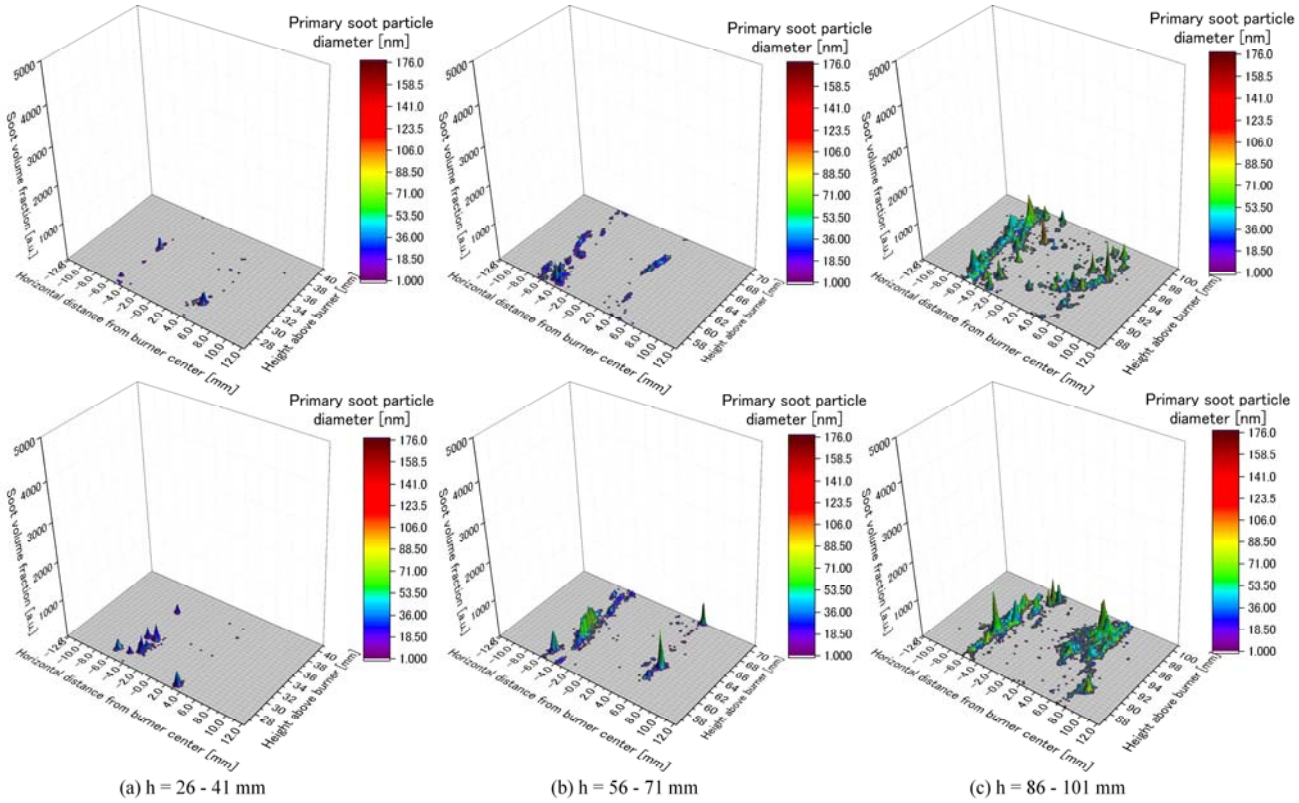

Fig. 7 Instantaneous two dimensional distributions of soot volume fraction and primary soot particle diameter for two different instants. The height indicates the soot volume fraction and the color indicates the primary soot particle diameter.

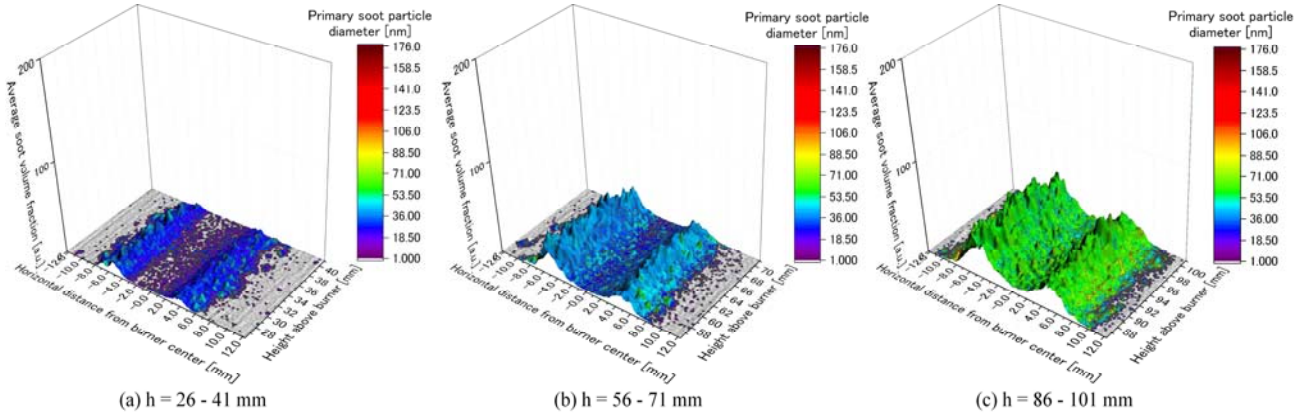

Fig. 8 Ensemble-averaged two dimensional distributions of soot volume fraction and primary soot particle diameter. The height indicates the soot volume fraction and the color indicates the primary soot particle diameter.

soot particle diameter distributions obtained by TiRe-LII are consistent with that obtained by SEM images. Since some LII signals of smaller particles obtained by the 1st camera are significantly decayed during the delay period between the 1st camera and 2nd camera (450 ns), such LII signals cannot be captured by the 2nd camera. Absence of the cumulative curves obtained by the TiRe-LII (the orange dashed curves) for smaller diameter region in the figure indicates such signals.

Figure 7 shows the instantaneous two dimensional distributions of the soot volume fraction and the primary soot particle diameter. From comparisons of two different instants for each *h*, it is found that the shapes and positions of soot regions are different between the two instants. This fact indicates the inhomogeneity of this combustion field. The inhomogeneity is considered to be caused by the turbulence and the fluctuation of the coal particle supplying rate. In the lower height above burner (Fig. 7 (a)), the regions where the soot can be observed are isolated and the primary soot particle diameter

[DOI: 10.1299/xxx.2014xxx000x]

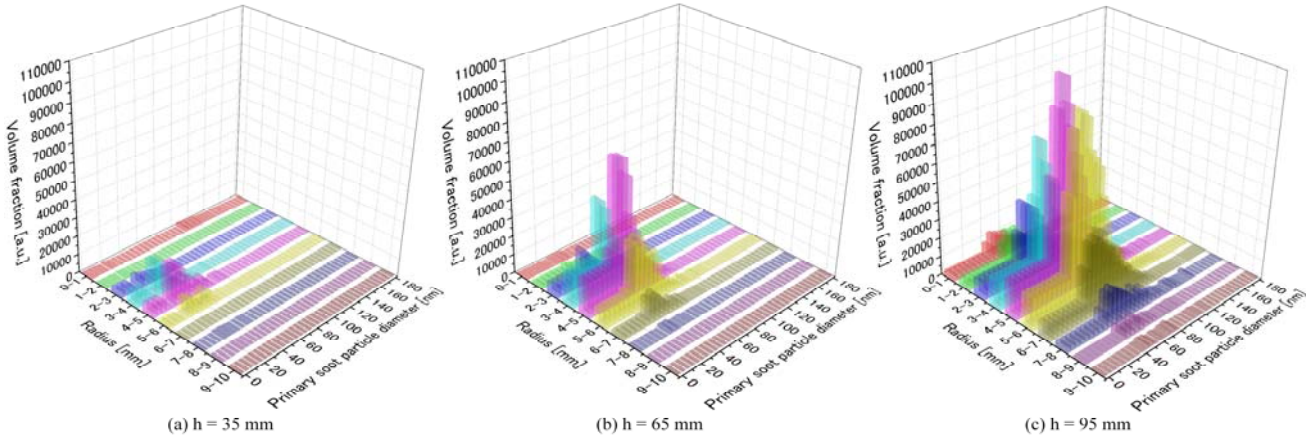

Fig. 9 Primary soot particle diameter distribution obtained by TiRe-LII for radial direction at (a) *h* = 35 mm, (b) *h* = 65 mm, and (c) *h* = 95 mm.

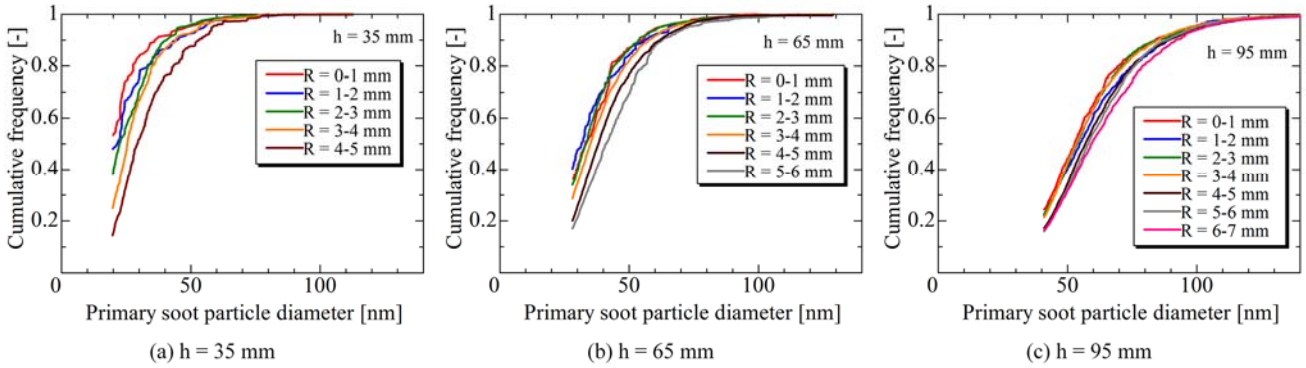

Fig. 10 Cumulative curves of soot particle diameter obtained by TiRe-LII for radial direction at (a) *h*=35 mm, (b) *h* = 65 mm, and (c) *h* = 95 mm.

is smaller than that in the higher *h*. As *h* increases (Fig. 7 (b) and (c)), the area of regions where the soot can be observed increases and the primary soot particle diameter also increases. The soot regions tend to unite and large united soot regions can be observed. However, the isolated small soot regions are still observed in the higher *h* (Fig. 7 (c)). This fact indicates that the soot formation characteristics in the coal combustion field is significantly different from the spray combustion field. The soot formation characteristics in the spray combustion field have been reported by some researchers (e.g., Oh and Shin (2006), Hayashi et al. (2011)). The large soot regions are formed in their spray flame, i.e., a number of isolated soot regions were not observed in their flame.

Figure 8 shows the ensemble-averaged two dimensional distributions of the soot volume fraction and the primary soot particle diameter. It is observed that on the whole, the primary soot particle diameter increases with increasing *h*. The soot region expands to both inner side and outer side with increasing *h*. However, the radial position of the peak value of soot volume fraction does not change significantly with increasing *h*.

Figure 9 shows the ensemble-averaged primary soot particle diameter distribution for radial direction obtained by TiRe-LII employing Eq. (3). The ensemble-averaged values were obtained from 500 TiRe-LII measurements. It is found that the peak value of soot volume fraction appears at the region with the radial distance of 4 – 5 mm from the burner center axis. In any radial distance, the soot particle diameter increases with increasing *h*. This trend indicates the growth of primary soot particle as the particles move to the downstream region. In addition to that, the distribution of soot volume fraction becomes wider with increasing *h*. Because the temperature around the central axis of the burner is lower than that in the region with radial position of 4 - 5 mm (Hashimoto et al., 2012b), the combustion reaction is not active around the center axis of the burner. Consequently, the soot volume fraction is low around the center axis of the burner. It is also found that the primary soot particle distribution does not change significantly for the radial direction in each *h*, although the soot volume fraction vary significantly for the radial direction.

Figure 10 shows the cumulative curves of soot particle diameter for radial direction obtained by TiRe-LII. The soot

[DOI: 10.1299/xxx.2014xxx000x]

particle diameter distribution shifts to larger side with increasing *h*, as also indicated in Fig. 9. It is found from Fig. 10 that the volumetric ratio of small particles is decreased with increasing radial distance at h = 35 mm. However, the variation of the primary soot particle diameter distribution along the radial direction is decreased with increasing *h*. This is caused by the mixing effect of the turbulence, i.e., the soot particles tend to disperse in the downstream region. Therefore, the variation of the primary soot particle diameter distribution becomes smaller in the downstream region because of the turbulent mixing effect.

4. Conclusions

In this study, the time-resolved laser induced incandescence (TiRe-LII) and the thermophoretic sampling (TS) methods were applied to the 4 kW coal jet burner to investigate the primary soot particle size distributions in a coal combustion field. The relative function between the signal decay ratio obtained by TiRe-LII and the primary soot particle diameter was defined based on the particle diameter distributions obtained from the SEM images of particles collected by TS. Employing the relative function, the spatial distributions of the primary soot particle diameter distributions were obtained.

The results show that the small isolated soot regions instantaneously exist in the entire combustion field. This characteristics is different from spray combustion field. From the ensemble-averaged TiRe-LII images, it was found that the maximum soot volume fraction is observed at the region with radial distance of 4 – 5 mm from the burner center axis. On the other hand the soot volume fraction around the burner center axis is low because of the low temperature. In any radial distance, the soot volume fraction and the primary soot particle diameter increases with increasing the height above the burner. It was also found that the volumetric ratio of small particles is decreased with increasing radial distance at the region close to the burner exit. However, the variation of the soot particle diameter distribution along the radial direction becomes smaller in the downstream region. This tendency is caused by the turbulent mixing effect.

It is expected that the accurate soot formation model will be developed by using the data obtained in this study.

Acknowledgements

Part of this work is supported by JSPS KAKENHI Grant Number 13351930.

References

Ahn, S., Watanabe, H., Shoji, T. and Umemoto, S., Numerical investigation of reaction kinetics of coal volatiles with a detailed chemistry and its simplification, Journal of Thermal Science and Technology, Vol. 11, No. 1 (2016), Paper No. 16-00017.

Aydin, O. and Durak, M.M., The effect of temperature distribution on tube rupture, Journal of Thermal Science and Technology, Vol. 7, No. 4 (2012) pp.753-766

Balusamy, S., Mustafa Kamal, M., Lowe, S.M., Tian, B., Gao, Y. and Hochgreb, S., Laser diagnostics of pulverized coal combustion in O_2/N_2 and O_2/CO_2 conditions: velocity and scalar field measurements, Experiments in Fluids, Vol.56 (2015), 108.

Cai, J., Handa, M. and Modest, M.F., Laser diagnostics of pulverized coal combustion in O_2/N_2 and O_2/CO_2 conditions: velocity and scalar field measurements, Combustion and Flame, Vol.162, Issue 4 (2015), pp.1550-1565.

Franchetti, B.M., Cavallo Marincola, F., Navarro-Martinez, S. and Kempf, A.M., Large Eddy simulation of a pulverised coal jet flame, Proceedings of the Combustion Institute, Vol.34, Issue 2 (2013), pp.2419-2426.

Hara, T., Muto, M., Kitano, T., Kurose, R. and Komori, S., Direct numerical simulation of a pulverized coal jet flame employing a global volatile matter reaction scheme based on detailed reaction mechanism, Combustion and Flame, Vol. 162, Issue 12 (2015) pp.4391-4407.

Hashimoto, N., Kurose, R., Tsuji, H. and Shirai, H., A numerical analysis of pulverized coal combustion in a multi-burner furnace, Energy & Fuels, Vol.21, Issue 4 (2007) pp.1950-1958.

Hashimoto, N., Kurose, R., Hwang, S., Tsuji, H. and Shirai, H., A numerical simulation of pulverized coal combustion employing a tabulated-devolatilization-process model (TDP model), Combustion and Flame, Vol. 159, Issue 1 (2012a), pp.353-366.

[DOI: 10.1299/xxx.2014xxx000x]

Hashimoto, N., Kurose, R. and Shirai, H., Numerical simulation of pulverized coal jet flame employing the TDP model, Fuel,Vol.97 (2012b), pp.277-287.

Hashimoto, N. and Shirai, H., Energy, Numerical simulation of sub-bituminous coal and bituminous coal mixed combustion employing TDP model, Vol.71 (2014), pp.399-413.

Hayashi, J., Watanabe, H., Kurose, R. and Akamatsu, F., Effects of fuel droplet size on soot formation in spray flames formed in a laminar counterflow, Combustion and Flame, Vol.158, Issue 12 (2011) pp.2559-2568.

Hayashi, J., Hashimoto, N., Nakatsuka, N., Tsuji, H., Watanabe, H., Makino, H. and Akamatsu, F., Soot formation characteristics in a lab-scale turbulent pulverized coal flame with simultaneous planar measurements of laser induced incandescence of soot and Mie scattering of pulverized coal, Proceedings of the Combustion Institute, Vol.34 (2013), pp.2435-2443.

Hwang, S., Kurose, R., Akamatsu, F., Tsuji, H., Makino, H. and Katsuki, M., Application of optical diagnostics techniques to a laboratory-scale turbulent pulverized coal flame, Energy & Fuels, Vol.19 (2005) pp.382-392.

Kurose, R., Makino, H. and Suzuki, A., Numerical analysis of pulverized coal combustion characteristics using advanced low-NOx burner, Fuel Vol.83 (2004) pp.693-703.

Muto, M., Watanabe, H., Kurose, R., Komori, S., Balusamy, S. and Hochgreb, S., Large-eddy simulation of pulverized coal jet flame - Effect of oxygen concentration on NOx formation, Fuel, Vol.142 (2015), pp.152-163.

Oh, K. C. and Shin H. D., The effect of oxygen and carbon dioxide concentration on soot formation in non-premixed flames, Fuel, Vol.85 (2006) pp.615-624.

Olenik, G., Stein, O.T. and Kronenburg, A., LES of swirl-stabilised pulverised coal combustion in IFRF furnace No. 1, Proceedings of the Combustion Institute, Vol.35 (2015), pp.2819-2828.

Rabacal, M., Franchetti, B.M., Cavallo Marincola, F., Proch, F., Costa, M., Hasse, C. and Kempf, A.M., Flamelet LES of a semi-industrial pulverized coal furnace, Proceedings of the Combustion Institute, Vol.35 (2015), pp.3609-3617.

Richter, H. and Howard, J.B., Formation of polycyclic aromatic hydrocarbons and their growth to soot-a review of chemical reaction pathways, Progress in Energy and Combustion Sciences, Vol. 26 (2000), pp.565-608.

Stein, O.T., Olenik, G., Kronenburg, A., Cavallo Marincola, F., Franchetti , B.M., Kempf, A.M., Ghiani, M., Vascellari, M. and Hasse, C., Towards comprehensive coal combustion modelling for les, Flow, Turbulence and Combustion, Vol.90 (2013), pp.859-884.

Sun, Z. W., Gu, D. H., Nathan, G. J., Alwahabi, Z. T. and Dally B. B., Single-shot, Time-Resolved planar Laser-Induced Incandescence (TiRe-LII) for soot primary particle sizing in flames, Proceedings of the Combustion Institute, Vol.35 (2015), pp.3673-3680.

Umetsu, H., Watanabe, H., Kajitani, S. and Umemoto, S., Analysis and modeling of char particle combustion with heat and multicomponent mass transfer, Combustion and Flame Vol.161 (2014) pp.2177-2191.

Vascellari, M., Schulze, S., Nikrityuk, P., Safronov, D. and Hasse, C., Numerical simulation of pulverized coal MILD combustion using a new heterogeneous combustion submodel, Flow, Turbulence and Combustion, Vol.92 (2014), pp.319-345.

Wen, X., Jin, H., Stein, O.T., Fan, J. and Luo, K., Large Eddy Simulation of piloted pulverized coal combustion using the velocity-scalar joint filtered density function model, Fuel, Vol.158 (2015), pp.494-502.

Zhao, X. and Haworth, D.C., Transported PDF modeling of pulverized coal jet flames, Combustion and Flame, Vol.161 (2014), pp.1866-1882.

[DOI: 10.1299/xxx.2014xxx000x]